Microstructure and Wear Properties of Al-Fe Surface Composites: Impact of Four Friction Stir Processing Passes

JMEPEG
https://doi.org/10.1007/s11665-026-14726-w

1059-9495/$19.00

ORIGINAL RESEARCH ARTICLE

Microstructure and Wear Properties of Al-Fe Surface Composites: Impact of Four Friction Stir Processing Passes

Behnoosh Sattari Baboukani, Morteza Shamanian, Sogand Abbaspoor-Zanjani, and Teresa Gatti

Submitted: 18 November 2025 / Revised: 28 February 2026 / Accepted: 10 May 2026

The number of passes during friction stir processing (FSP) can influence the microstructure and wear properties of thin metallic films. In this study, thin Aluminum-Iron (Al-Fe) films are deposited on a low carbon steel substrate via a plasma spray process with an initial coating thickness of approximately 100 μm. The effect of FSP pass numbers on the microstructure evolution at the stir zones (SZs) and heat-affected zones (HAZs) is investigated using optical microscopy and electron backscatter diffraction (EBSD) techniques. The study also investigates surface wear behavior by conducting a reciprocating wear test (1000 m sliding distance under 15 N load) and utilizing scanning electron microscopy (SEM) to examine the topography of worn surfaces, revealing that the wear track depth decreased from approximately 160 μm in the As-sprayed coating to 152, 120, 18, and 20 μm after one to four FSP passes, respectively. The films were analyzed using X-ray diffraction (XRD), which revealed the formation of Fe-Al intermetallic compounds in all of the surface composites. Applying the second pass of FSP led to the formation of the Widmanstätten ferrite plates from recrystallized austenite grains, both at the stir zones (SZs) and the heat-affected zones (HAZs). The grains underwent thickening and elongation as a result of an increased diffusivity of carbon and higher heat inputs applied to the surface, which occurred with an increase in pass numbers. Applying additional FSP passes led to a more anisotropic microstructure, which was attributed to the accumulation of a higher number of dislocations. Conducting multiple FSP passes (three or four) has improved the wear resistance and reduced the running-in distance in friction coefficient measurements, leading to a reduction in total wear rate from 1.6 $\times 10^{-2}$ μm m^{-1} in the As-sprayed condition to 0.15 and 0.17 $\times 10^{-2}$ μm m^{-1} after three and four passes, respectively. Correspondingly, the Vickers microhardness of the stir zone increased from 198 HV in the As-sprayed coating to 405 HV after four passes, while friction coefficients remained in the range of 0.33-0.42. An analysis of the wear track revealed a shift from adhesive wear to abrasive wear as the number of FSP passes increased.

Keywords friction stir processing, intermetallic, recrystallized austenite, widmanstätten ferrite

1. Introduction

Friction Stir Processing (FSP) is a technique used to fabricate surface composites (Ref 1) and/or to modify the microstructure of the metallic surfaces (Ref 2–4). To create surface composites using the FSP method, various techniques have been employed to introduce reinforced particles into the surface. Examples of these techniques include adding particles into machined grooves (Ref 5) on target plates or incorporating reinforcement particles through drilled holes (Ref 6). However, these methods often suffer from the issue of reinforcement particles flashing out during FSP, which can limit the improvements in mechanical and tribological properties (Ref 7). The emerging technique of applying FSP on spray-coated surfaces has been shown to reduce the loss of reinforcement particles, resulting in dense surface structures that can improve thermal conductivity and mechanical properties (Ref 8). Using multi-pass FSP, Paidar et al. (Ref 9) investigated the effect of post-processing on 10-cycle accumulative roll bonded Al-2%B_4C composites. Increasing the number of tool passes from 1 to 8 significantly enhanced the homogeneity and fragmentation of B_4C particles, resulting in improved mechanical and tribological properties. Consequently, the tensile strength increased from 86.84 to 173.92 MPa, while the wear rate decreased from 6.198 $\times$ 10^{-5} to 1.095 $\times$ 10^{-5} mm^3/Nm. In another study, Morisada et al. (Ref 10) were able to modify thermally sprayed WC-CrC-Ni films and achieve a significant increase in hardness for the processed films, thanks to the mechanical substrate-coating interlocking effect. Additionally, Li et al. (Ref 11), produced Al_2O_3/TiO_2 reinforced particles on a copper substrate using plasma spraying and observed that a uniform distribution

Supplementary Information The online version contains supplementary material available at https://doi.org/10.1007/s11665-026-14726-w.

Behnoosh Sattari Baboukani, Department of Materials Engineering, Isfahan University of Technology, Isfahan 8415683111, Iran; and Department of Mechanical Engineering, University of California, Berkeley, CA 94720; **Morteza Shamanian**, Department of Materials Engineering, Isfahan University of Technology, Isfahan 8415683111, Iran; and **Sogand Abbaspoor-Zanjani** and **Teresa Gatti**, Department of Applied Science and Technology, Politecnico di Torino, 10129 Turin, Italy. Contact e-mail: sogand.abbaspoor@polito.it.

Published online: 08 August 2026

of particles in the matrix and grain refinement resulted in a four-fold increase in film hardness for surfaces subjected to three friction stir passes compared to an unprocessed copper surface. Surface composites have been developed by incorporating ceramic particles into various metallic surfaces using FSP, and more recently, it has been shown that the presence of the ceramic particles can improve the mechanical (Ref 10–13) and tribological (Ref 11, 14, 15) performance of such composites. For instance, Pol et al. (Ref 12) incorporated TiB_2 and B_4C ceramic particles into the AA7005 alloy surface using FSP, resulting in a 70 HV increase in surface hardness compared to the base alloy. The uniform distribution of B_4C nanoparticles achieved after the FSP was also found to impact the wear resistance and surface durability of the AA7075-T6 alloy (Ref 13). In another study, Yang et al. (Ref 16) investigated the fabrication of AA5083/316 stainless steel surface composites via FSP, demonstrating that multi-pass FSP significantly refined the grain structure (from 7.02 to 5.89 μm), improved the dispersion of 316 stainless steel particles within the aluminum matrix, and consequently enhanced the mechanical properties, wear resistance, and corrosion performance of the modified surface layers.

The high local temperature and the plastic deformation that occurred during the FSP results in the reaction between the particles and the embedded matrix and hence leads to the formation of the in situ intermetallic compounds. The intermetallic compounds produced via this method usually have fine structures with an improved interfacial bonding with the embedded matrix. Further, they are homogeneously dispersed in the composites' matrix leading to an increase in the thermal stability of these phases at elevated temperatures and an improved mechanical behavior. For instance, the in situ formation of Al_2Cu intermetallic compounds was observed after applying FSP on the aluminum alloy surface composited with high entropy AlCoCrFeNi particles resulting in a significant decrease in the wear rate of the surface (Ref 17). Al_3Ni intermetallic particles were also formed after applying FSP onto the aluminum matrixes, resulting in a noticeable increase in microhardness (Ref 18). Incorporating 34CrNiMo6 powder into the AA2024 alloy using FSP has also led to the formation of $Al_{13}Fe_4$ intermetallic compounds with a uniform dispersion resulting in a five-fold increase in the surface hardness (Ref 19).

Extensive research has investigated the impact of various FSP parameters such as rotational and traverse speed of the FSP machine, the geometry and the tilt angle on microstructure evolution and surface mechanical properties of different alloys and composites. In addition, although receiving comparatively less attention in research, the number of FSP passes is also an important factor that affects the surface's microstructure and mechanical characteristics. For example, Heidarpour et al. (Ref 20) investigated the effect of FSP pass number on the surface of Cu/TiO_2 nanocomposites and found that mechanical properties of the surface composite including microhardness, yield and tensile strength improved by increasing the pass number. Singhal et al. (Ref 21) optimized FSP parameters for AA 5083-H111/Al-Fe composites using a Taguchi L27 design and identified a tool shoulder diameter of 21 mm (at 900 rpm and 63 mm min^{-1}) as optimal, achieving refined grain structure and an ultimate tensile strength up to 84% of the base material strength. Similarly, Saravanakumar et al. (Ref 22) reported that FSP of AA2024 reinforced with SiC nanoparticles, optimized at 1000 rpm (with 10 kN and 40 mm min^{-1}), improved microhardness (120 HV) and enhanced wear resistance due to grain refinement and uniform dispersion with strong interfacial bonding of SiC particles within the aluminum matrix. Moreover, Senthilkumar et al. (Ref 23) also showed that increasing the FSP pass number with a specific rotational speed, reduced the tunnel void at the stir zone (SZ) on the surface of the AA6082 alloy, results in an enhancing tensile and impact strength of the surface. In our previous study, we showed that the wear rate of a low carbon steel has decreased by an order of magnitude using more FSP passes applied to the surface (Ref 2).

The present study aims to investigate the influence of varying FSP pass numbers (up to four) on the microstructure, hardness, and wear resistance of Al-Fe surface composites. To this end, a mixed powder of Al-30 wt.% Fe is plasma-sprayed onto a low carbon steel substrate, and the evolution of compounds and the composite cross sectional microstructures during each FSP pass is examined. Additionally, two as-sprayed specimens undergo heat treatment to obtain Al-Fe intermetallic compounds, and their tribological behavior is compared to that of the friction stir-processed samples under the same conditions. To the best of our knowledge, while previous studies have focused on various metallic systems, a specific investigation into the evolution of Al-Fe intermetallic compounds through the combination of plasma spraying and multiple FSP passes remains unexplored. This work provides a detailed analysis of how the number of FSP passes dictates the phase transformation from Al-rich to Fe-rich intermetallic in this specific composite system.

2. Materials and Methods

A low carbon steel plate (chemical composition is given in Table 1) with a thickness of ~ 5 mm has been used as the base materials (substrate) in this study. The plate has been cut into 6 smaller samples with the dimensions of 15 ×4 cm^2. Magnetic grinding was initially employed to remove oxide films and other contaminations from the surface of these substrates. Further, sand-blasting has been utilized in order to improve the mechanical interlocking and the adhesion energy between the surface and the films which were deposited later. The plasma spraying parameters summarized in Table 2 were selected based on the optimized conditions reported in our previous studies (Ref 2, 24), where Al-30 wt.% Fe powders were successfully deposited onto low carbon steel substrates with a coating thickness of approximately 100 μm. The selected current,

Table 1 Chemical composition of studied low carbon steel, wt.% (Ref 2, 24)

Element	C	Mn	Ni	Cr	Si	P	S	Fe
Mass fraction	0.0397	0.8530	0.0477	0.0109	0.0101	< 0.0080	< 0.0050	Rem.

Table 2 Plasma spraying parameters of the Al-Fe coating (Ref 2, 24)

Powder composition (wt.%)	Current, A	Voltage, V	Main air flow Ar, L/min	Carrier air flow N_2, L/min	Powder feed rate, g/min	Traveling speed, mm/s	Spraying distance, mm
Al-30%Fe	500	40	30	5	35	1000	90

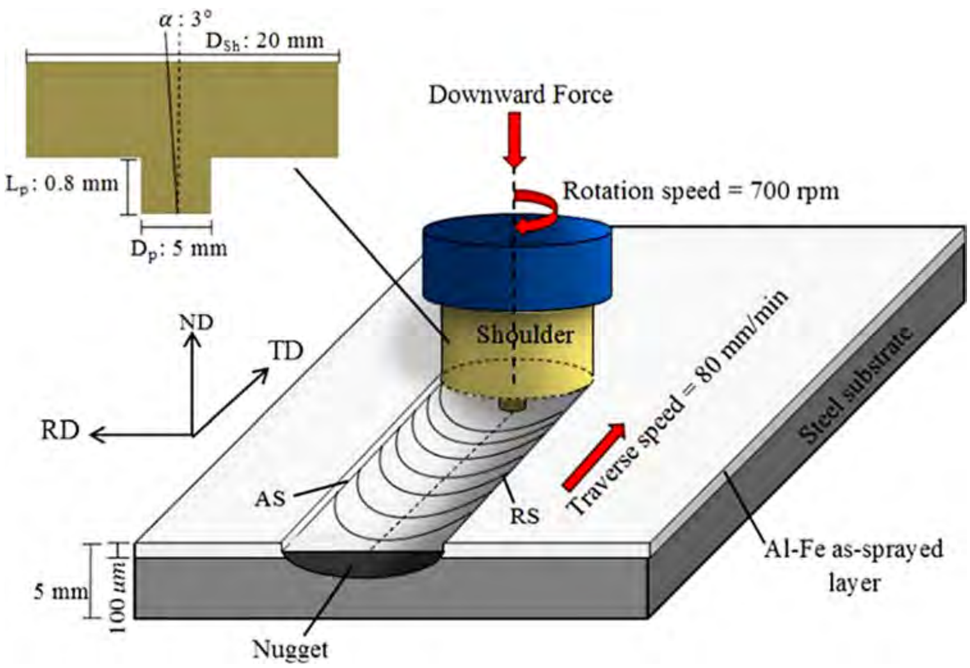

Fig. 1 Schematic illustration of FSP tool and setup

voltage, gas flow rates, powder feed rate, spraying distance, and traverse speed were shown in our previous studies to produce a uniform and adherent coating prior to friction stir processing. These parameters were therefore adopted in the present work to ensure reproducibility and direct comparability of the microstructural evolution and phase formation during subsequent FSP passes. The Fe powders used in this study were commercially pure and had an irregular shape, with a size distribution ranging from approximately 143-480 μm. In contrast, the Al powders had a rounded structure and a size distribution of approximately 6-57 μm (see supplementary Fig. S1).

Subsequently, the Al-Fe surface composites were fabricated using FSP, whereby the Al-Fe coated film on the steel substrate was stirred. This study employed a tungsten carbide stir tool, which featured a cylindrical pin with a diameter of 5 mm and was attached to a 20 mm shoulder, for carrying out FSP. The pin was designed to penetrate the substrate almost vertically, reaching a depth of $\sim$ 0.8 mm. As such, the aim was to achieve a homogeneous distribution of reinforcement particles within the steel matrix, resulting in a volume fraction of approximately 10%. The fabrication of the surface composites involved the utilization of a tungsten stir tool, which rotated clockwise at a speed of 700 rpm and traversed the surface at a speed of 80 mm/min. To prevent defects such as flashing and keyhole caused by the pin, a tool angle (α) of 3° was employed (Ref 25). The schematic of the FSP process used in this study is shown in Fig. 1. In order to study the impact of the number of passes on the structure and tribological properties of the surface composites, one to four unidirectional FSP passes were applied on the Al-Fe-coated steel substrates using constant rotation and traverse speeds.

To compare the tribological properties and phase transformation of the FSP-fabricated surface composites with those of the as-sprayed Al-Fe-coated steel, two samples were heat-treated at 900 °C using a RHF 1400 programmable furnace. The samples were subjected to heat treatment for one and 2 h at a rate of 50 °C/min and were then quenched in ambient temperature. The tribological behavior of these samples was then compared to that of the FSP-fabricated surface composites.

The cross section of the FSPed samples were mounted and mechanically grounded up to 2400 girt using SiC papers, and polished with 0.5 μm alumina suspension. Afterward, they were etched in 2% Nital solution for about 10 s to observe grain features. Optical microscopy, X-ray diffraction (XRD, PHILIPS XPERT- MPD, Cu K_α radiation), scanning electron microscopy (SEM, PHILIPS XL30) and electron back scatter diffraction (EBSD, Oxford AZtec) were employed for microstructural characterization and phase evolution. Vickers micro-hardness profiles using a load of 5 N and a dwelling time of 10 s were measured on the cross section of the samples, perpendicular to the traverse direction of the FSP, using a Buehler LTD tester. The measurements were taken at $\sim$ 200 μm below the processed surface, with a distance of 300 μm between two consecutive measurements. The wear behavior was measured using a reciprocating tester made by an

Table 3 Wear test (reciprocating) parameters (Ref 2)

Pin	Pin shape	Pin diameter, mm (concave head)	Sliding velocity, cm s^{-1}	Applied force, N	Total sliding distance, m	Temperature, °C
AISI 52100	Cylindrical	5	10	15	1000	25 ±2

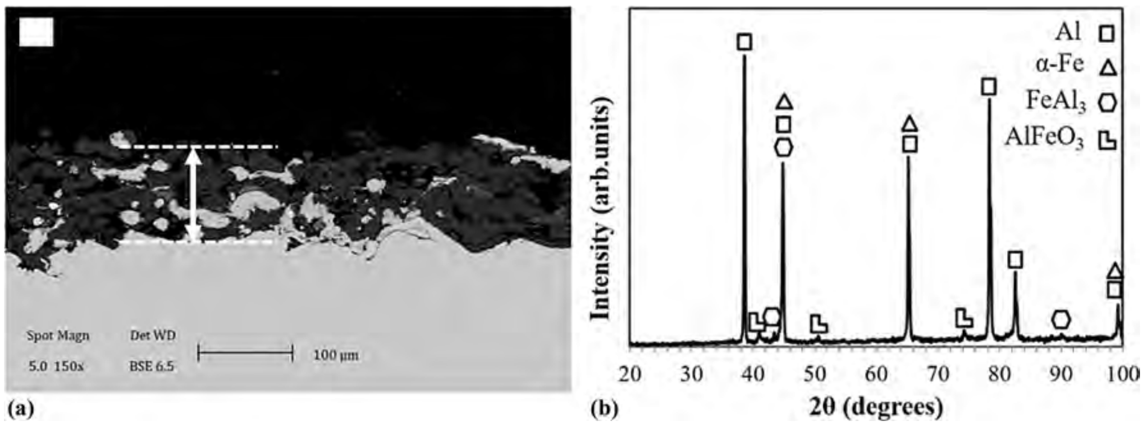

Fig. 2 (a) Al-30 wt.% Fe as-sprayed coating on the low carbon steel, (b) XRD scan of the Al-Fe surface coating on the low carbon steel substrate

AISI 52100 pin (hardness ~ 850 HV). The FSPed samples' surfaces were grounded by SiC papers and cleaned by acetone and the wear behavior of the middle sections, at which the tool pin was traversed during FSP (showed with dashed lines in Fig. 1), was investigated using the parameters listed in Table 3. Friction coefficients and mass loss for each sample were measured. Worn surfaces were also imaged by SEM in order to study the dominant wear mechanism. Subsequently, the surface roughness (R_a) and the total wear depths were measured using a profilometer (Mitutoyo). Hence, the total wear rate in the track is calculated by Eq 1:

$$\text{Wear rate} = \text{Volume loss}/\text{Sliding distance}\left(\text{mm}^3\text{m}^{-1}\right) \quad \text{(Eq 1)}$$

3. Results and Discussion

3.1 Phase Analysis

As illustrated in Fig. 2(a) the Al-Fe coating has a thickness of 100 μm on the low carbon steel substrate. The XRD spectrum of the Al-Fe surface coating shows that aluminum and ferrite are major phases in this layer (Fig. 2b).

Figure 3(a) and (b) displays the XRD spectra of various FSP-processed and heat-treated samples, respectively. The surface composites that underwent one to four FSP passes showed the presence of Fe-Al intermetallic compounds, as indicated in the XRD spectra presented in Fig. 3(a). The formation of intermetallic compounds due to the strong interactions between Al and Fe is a well-known phenomenon. Previously, the formation of intermetallic compounds during dissimilar friction stir welding (FSW) of aluminum alloys to steels (Ref 26, 27) as well as on FSP-fabricated Al-Fe composites (Ref 27) has been reported, owing to the strong interactions between Al and Fe. The high reaction rates observed between Al and Fe can be attributed to the heat released from exothermic reactions between Al and transition metals (Ref 28), as well as the high local heat generated during the FSP process. Further, FSP is a thermo-mechanical process which generates severe plastic deformation (SPD) and promotes the reaction between Al and Fe (Ref 27). The XRD analysis revealed that the surface composite fabricated with one FSP pass had major compounds of $Al_{13}Fe_4$ and Al_5Fe_2. However, with an increasing number of FSP passes, other intermetallic compounds such as Fe_3Al and Al_5Fe_2 were also formed, as shown in the XRD spectrum of the surface composite subjected to four FSP passes in Fig. 3(a). Fe-Al binary phase diagram indicates the presence of five intermetallic compounds that remain stable, namely FeAl, Fe_3Al, $FeAl_2$, Fe_2Al_5, and $FeAl_3$ (Ref 26, 28). The findings of this study indicate that increasing pass number results in the creation of Al-Fe intermetallic compounds that are comparatively more stable. The solid interface between Al and Fe is known to trigger the precipitation of intermetallic compounds with higher Al content, based on the kinetic and thermodynamic driving forces (Ref 29). This research has demonstrated that the stress and heat input applied during the first pass of FSP were capable of creating intermetallic compounds with a higher concentration of Al. On the other hand, the formation of Fe-rich intermetallic compounds required more thermal energy (Ref 30). Indeed, the additional heat input and stress generated by increasing pass number, drives the formation of Fe-rich intermetallic compounds.

The XRD patterns shown in Fig. 3(a) reveal that the intensity of Fe-Al intermetallic compounds increased as the number of passes was incremented from two to four. An

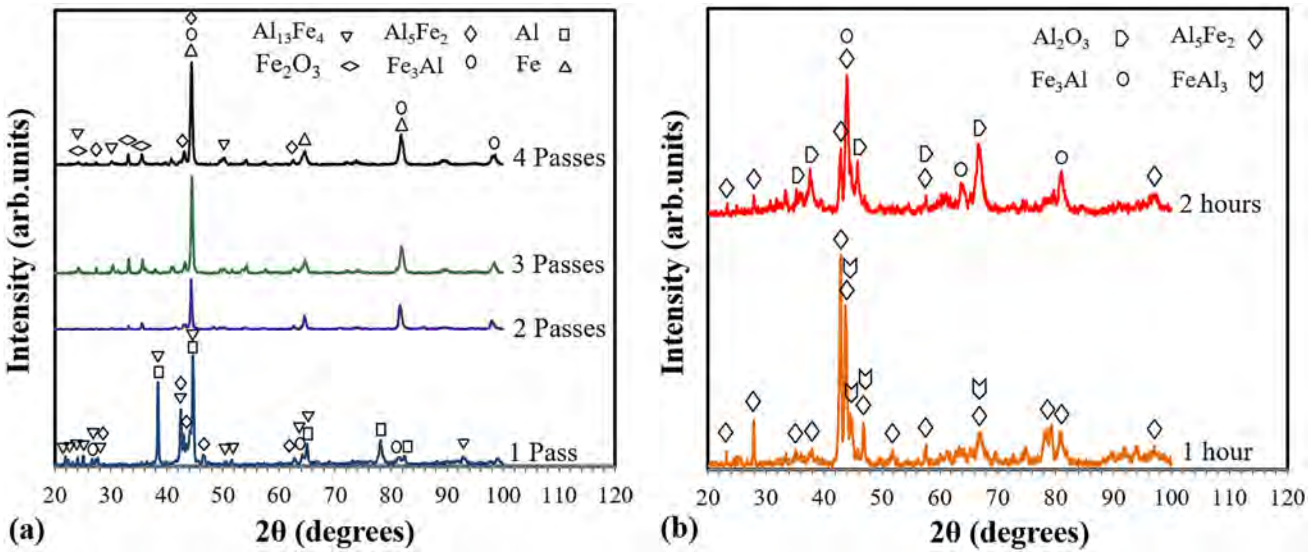

Fig. 3 XRD patterns of: (a) Al-Fe FSPed surface composites fabricated via different number of passes, (b) heat-treated Al-30 wt.% Fe as-sprayed coatings on the low carbon steel substrate

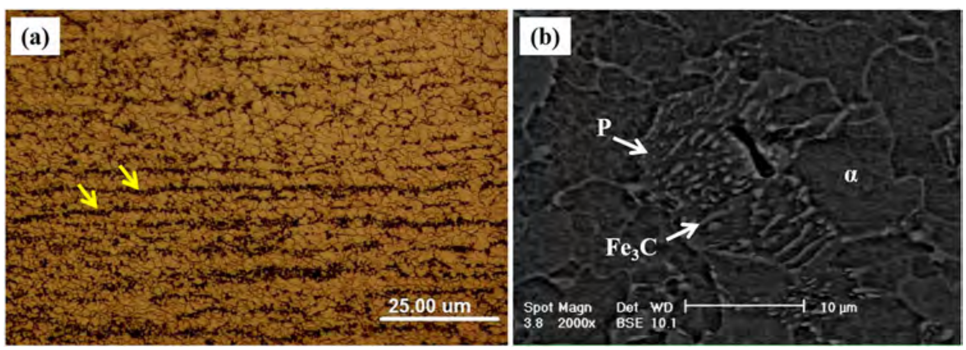

Fig. 4 (a) Optical image of the ferritic-pearlitic microstructure of the low carbon steel used as the base material in this study, (b) SEM image of the lamella microstructure of one of the pearlite colonies

increase in the number of passes resulted in an improvement in the distribution of reinforcement particles, which in turn enhanced the Al-Fe interfacial surface. As a result, the reactions between the two elements became more substantial and the formation of intermetallic compounds is enhanced. Furthermore, with an increase in the number of passes to two or more, the diffraction peaks corresponding to Al vanished, indicating a complete conversion of Al to Al-Fe compounds. Therefore, the sample processed with four passes showed the best performance promoting the formation of stable Fe-rich intermetallic compounds, improved reinforcement particle distribution, enhanced the Al-Fe interfacial area, and led to complete conversion of Al to intermetallic phases.

Based on the XRD pattern depicted in Fig. 3(b), subjecting the coated samples to a 1 h heat treatment at 900 °C was sufficient to create the Al_5Fe_2 compound. Furthermore, when the sample was subjected to a 2 h heat treatment at the same temperature, XRD analysis detected Fe-rich intermetallic compounds like Fe_3Al as well as aluminum oxides.

3.2 Microstructure Evolution

Figure 4(a) shows the microstructure of the low carbon steel used as the base material in this study. This microstructure consists of equiaxed ferrite grains with the average size of 2.7 ± 0.4 μm and banded pearlite islands. The flattened ferrite grains and planar pearlite colonies are characteristics of warm-rolled steels which result in anisotropic mechanical properties of the steel (Ref 29, 30). This abnormal segregation is attributed to the hyper-dispersion of the alloying elements, especially Manganese (Ref 31). The yellow arrows in Fig. 4(a) indicate the dark regions, which correspond to the fine lamellar colonies of pearlite present in the microstructure. A higher magnification SEM image of a pearlite colony is displayed in Fig. 4(b).

The cross sectional microstructures of the FSPed surface composites at different regions are illustrated in Fig. 5 (also supplementary Fig. S2). For the single-pass FSPed sample, the HAZ contained two regions: the inter-critical-heat-affected zone (ICHAZ) and fine-grained heat-affected zone (FGHAZ). ICHAZ, which is near the base metal, contains ferrite grains and pearlite colonies in the banded structures, as seen in Fig. 5(d) and (e). Ferrite grains in this region are smaller than the ferrite structure in the base metal. The microstructure provides evidence that the temperature in this region dropped below Ae_3, resulting in the presence of both austenite and ferrite phases within the structure. Upon cooling to the room

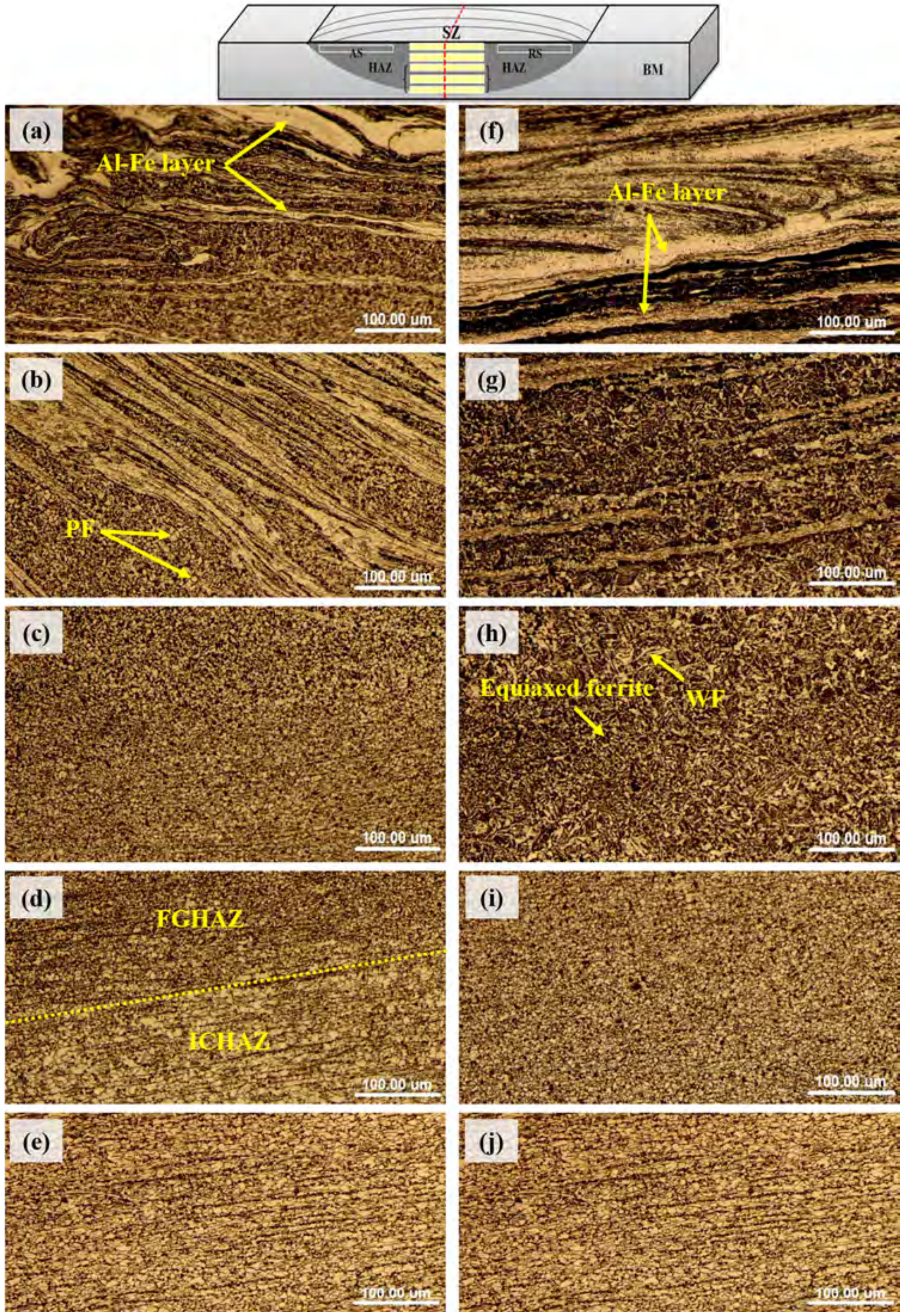

Fig. 5 Microstructure of the stir zone : (a) and (b) 1 FSP pass, (f) and (g) 2 FSP passes, (k) and (l) 3 FSP passes, (n) and (o) 4 FSP passes, the coarse-grained heat-affected zone (CGHAZ) :(h) 2 FSP passes, (m) 3 FSP passes, (p) 4 FSP passes, the fine-grained heat-affected zone (FGHAZ): (c) and (d) 1 FSP pass, (i) 2 FSP passes, and the inter-critical affected zone (ICHAZ): (d) and (e) 1 FSP pass, (j) 2 FSP passes, (AF: Allotriomorphic Ferrite, PF: Polygonal Ferrite, WF: Widmanstätten Ferrite, P: Pearlite)

temperature, the microstructure underwent a transformation to fine ferrite grains and pearlite colonies.

The microstructure of the fine-grained heat-affected zone (FGHAZ) for the single-pass FSPed sample is depicted in Fig. 5(c) and (d). This region, located near the stir zone, is characterized by fine ferrite grains and pearlite colonies. During FSP, the FGHAZ was exposed to the austenitization temperature beyond Ae_3. Subsequently, the austenite grains were decomposed into small ferrite grains and pearlite colonies upon cooling to room temperature. Figure 5(a) and (b) illustrates that the microstructure of the stir zone (SZ) is predominantly composed of equiaxed fine ferrite grains, small colonies of pearlite, and a minor fraction of polygonal ferrite grains. The formation of these small grains is indicative of dynamic recrystallization (DRX), a typical phenomenon that occurs during FSP. Despite the peak temperature of this region

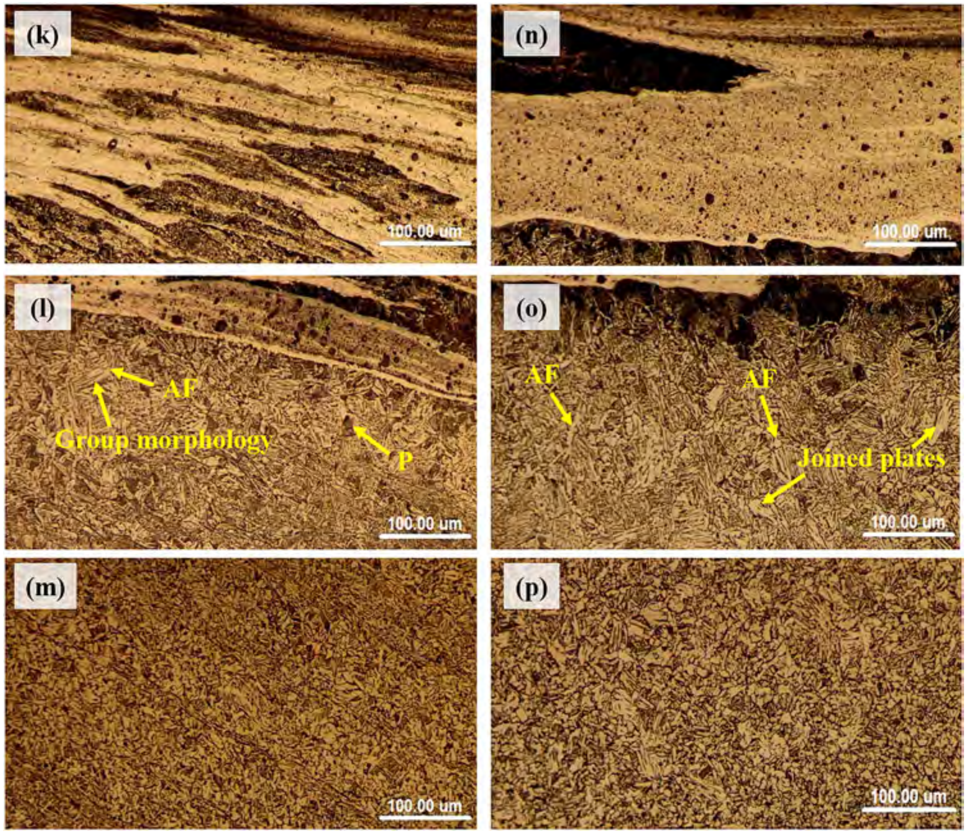

Fig. 5 continued

exceeding that of the FGHAZ during FSP, the pinning effect resulting from the Al-reinforced particles prevented grain growth in this area. Microstructures of HAZ after the second, third, and fourth FSP passes exhibit three regions: ICHAZ, FGHAZ, and coarse-grained HAZ (CGHAZ), as depicted in Fig. 5 (and also refer to supplementary Fig. S2). The presence of polygonal, allotriomorphic, and Widmanstätten ferrites characterized the microstructure of CGHAZ in these samples. Typically, Widmanstätten ferrite exhibits a grouping morphology where several plates of ferrite are formed from one allotriomorph in the same direction (Ref 32), and this morphology was observed in the CGHAZ microstructure. The microstructures observed in this study are reminiscent of those reported for dissimilar Friction Stir Welding (FSW) joints between mild steel and Ni-based alloy 625 (Ref 33). The microstructures of the SZs and CGHAZs in the samples subjected to two, three and four FSP passes were found to be similar to each other, while Widmanstätten ferrite grains had thicker and longer planes in the SZs (in comparison with their CGHAZ). By increasing pass number, Widmanstätten ferrite plates became thicker and longer both in SZ and CGHAZ. These plates probably widened because of the increased diffusivity of C in ferrite. By increasing pass number, FSPed samples have been subjected to a high temperature for a longer time. The mean diffusion distance ($X\overline{C}$) increased according to the Eq 2:

$$\overline{X} = \sqrt{Dt} \quad \text{(Eq 2)}$$

where D is the carbon diffusion coefficient in ferrite and t is time (Ref 32–34). Furthermore, as the number of FSP passes increased, the pre-heating process from the previous passes led to higher temperatures in the samples. Each sample reached a temperature of around 500 °C before the next FSP pass was conducted. The increase in temperature was found to enhance the diffusivity (Ref 32, 34).The Widmanstätten ferrite plates in the SZ exhibit a narrower width, and the volume fraction of this phase is greater in the SZ compared to the CGHAZ, as demonstrated by Fig. 5. This trend holds true for samples that have undergone two, three, and four passes of FSP. The elongation of the Widmanstätten plates was observed as the number of passes increased from two to three. The observed phenomenon can be attributed to the anisotropy of the Al interface (Ref 33). Additionally, the anisotropic elastic strain energy arising from the mismatch in lattice parameters between the newly precipitated phase and the parent matrix (Ref 35) also plays a role. Severe plastic deformation is imparted on the samples during FSP, and this deformation is intensified with an increase in the number of passes. This leads to a greater degree of interfacial anisotropy. As the anisotropy increases, the rate of plate elongation also increases, resulting in sharper edges of the plate (Ref 36). Moreover, the presence of Al-Fe reinforced particles further increases the lattice mismatch between the Widmanstätten plates and austenite grains. However, the formation of hard ceramic Fe-Al particles after a higher number of FSP passes contributes to enhanced dislocation density by pinning the grain boundaries (Ref 37). This can potentially halt the widening of the Widmanstätten plates in SZs due to the formation of harder Fe-Al intermetallic components for the sample subjected to four FSP passes. Interface mobility is a crucial factor in plate elongation (Ref 38). However, as the density of dislocations increases, the migration capability of the interface decreases. Figure 5(n) and (o) illustrates the presence of fine Widmanstätten plates in the SZs for samples that underwent the third and fourth passes of FSP. The disappearance or joining of adjacent plates at the SZ, as seen in Fig. 5(n), can result in a decrease in the elongation rate between the third and fourth passes. The FSPed samples in this study did not exhibit a thermo-mechanically affected zone (TMAZ) because of the allotropic transformation that occurred in these regions due to natural cooling to room temperature. Therefore, there is no specific region that experiences significant plastic deformation. The absence of a TMAZ in similar and dissimilar FSW jointed steels has also been reported in several studies (Ref 33, 37).

The microstructures of the advancing side (AS) and retreating side (RS) for different FSPed samples are shown in Fig. 6. The AS microstructure for all samples subjected to different numbers of FSP passes contains fine equiaxed ferrite grains. The RS microstructure of the single-pass FSPed sample is almost identical to its AS microstructure. However, with an increase in the number of passes, Widmanstätten plates are formed, and the volume fraction of this phase increases. The microstructure of the RS in the third and fourth FSP passes shows the presence of fine polygonal ferrite and Widmanstätten plates on top of the stirred layer, as depicted in Fig. 6. This layer is formed as a result of extreme shear stress caused by the axial force applied during FSP (Ref 39).

To examine the microstructure of the base metal and the SZ of the sample treated with four FSP passes, electron backscatter diffraction (EBSD) was employed. The image quality (IQ) map (Fig. 7) displays the crystallographic regions and grain boundaries in bright and dark colors, respectively, as indicated by the contrast variations. The base metal's microstructure comprises equiaxed ferrite grains (Fig. 7a). The SZ, on the other hand, contains a mixture of polygonal ferrite and long

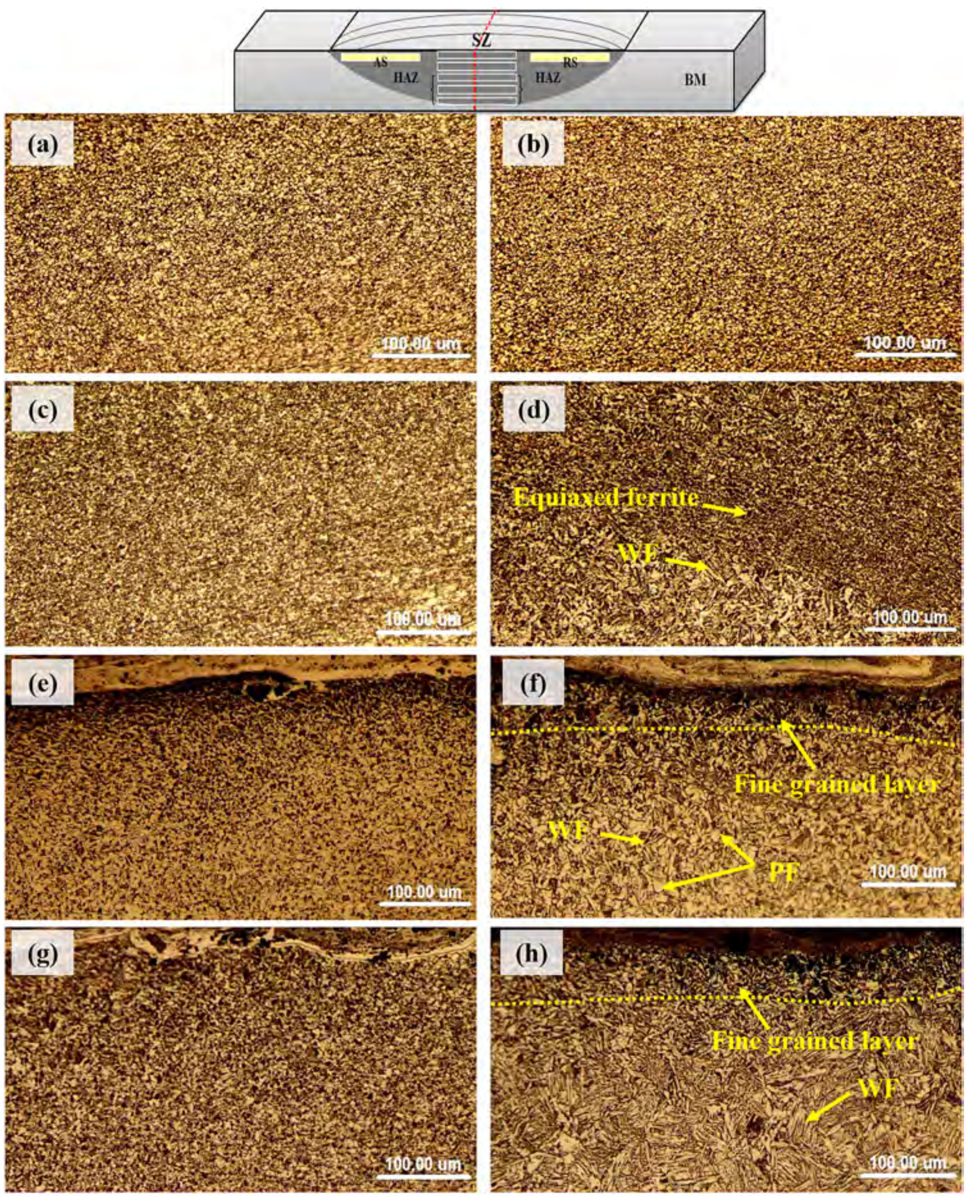

Fig. 6 Microstructure of stir zone in advancing side (AS) for the surface composite fabricated by: (a) 1 FSP pass, (c) 2 FSP passes, (e) 3 FSP passes, (g) 4 FSP passes, and retreating side (RS) for the surface composite fabricated by: (b) 1 FSP pass, (d) 2 FSP passes, (f) 3 FSP passes, and (h) 4 FSP passes

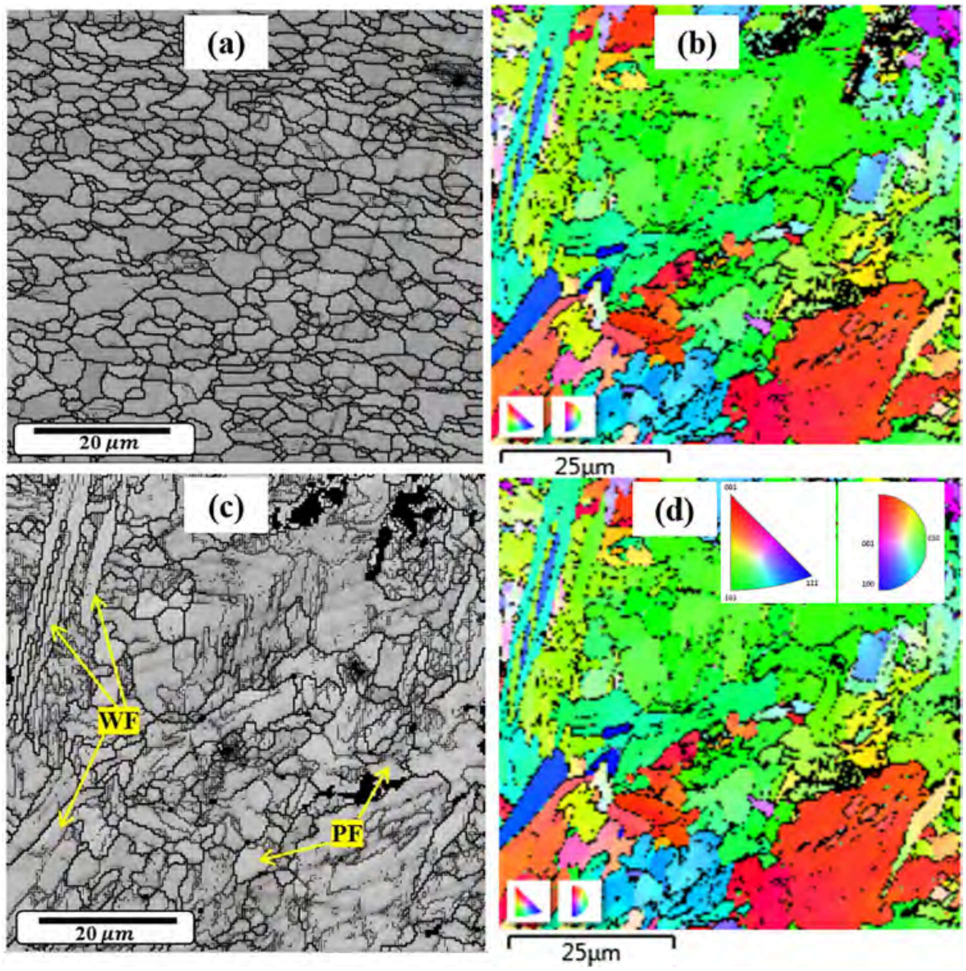

Fig. 7 Application of EBSD analysis to characterize the microstructure, (a) image quality (IQ) map of the base metal, (b) inverse pole figure (IPF) of the base metal, (c) IQ map of the SZ in sample which subjected to 4 FSP passes, and (d) IPF of the SZ in sample which subjected to 4 FSP passes

plates of Widmänstatten, as depicted in Fig. 7(c). To determine the microstructure's texture, inverse pole figure (IPF) maps were used to represent the distribution of crystallographic orientations based on the reference direction. Figure 7(b) illustrates that the low carbon steel employed in this study exhibits a random crystallographic distribution. However, in the sample subjected to four FSP passes, most of the grains in the SZ are oriented in the (101) plane (Fig. 7d).

3.3 Micro-hardness

Figure 8 presents the mean micro-hardness of the SZs for different surface composites, while Fig. S3 shows the Vickers micro-hardness measured on the cross section of different FSPed samples. Compared to the as-sprayed surface, the single-pass FSPed surface exhibits an increase of approximately 50 HV in Vickers micro-hardness. The inhomogeneous distribution of hardness values indicates the formation of intermetallic compounds on the surface composites. The sample that underwent four FSP passes exhibited the highest overall hardness (405 HV) among all surface composites. This value was almost twice as high as that of the as-sprayed substrate (198 HV). As described earlier, the formation of Widmanstätten plates of ferrite occurred after the second FSP pass, and their volume fraction increased with each subsequent pass.

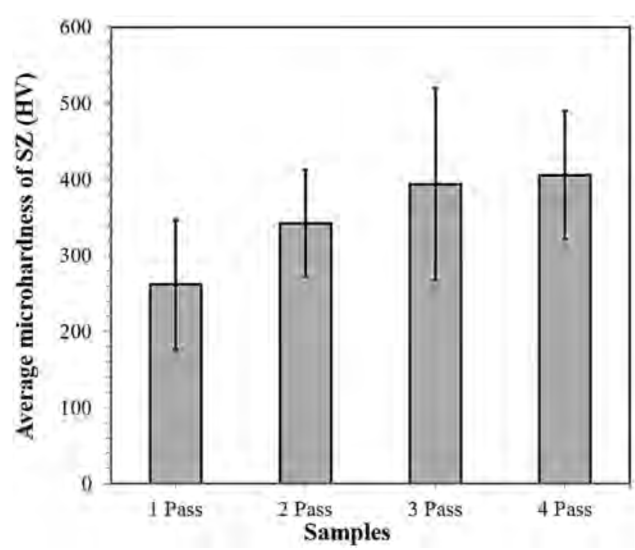

Fig. 8 Mean micro-hardness of the SZs in different samples error bars in illustrate standard deviation in the micro-hardness of the SZs

The increased volume fraction of the Widmanstätten ferrite phase formed after the second FSP pass could be responsible for the higher overall hardness observed in samples with more FSP passes. Furthermore, as depicted in Fig. 3(a), multiple passes result in the formation of Fe-rich intermetallic compounds, with the intensity of these phases increasing with each pass. These compounds exhibit higher hardness compared to their Al-rich counterparts. Overall, the sample processed with four FSP passes exhibited the highest hardness (405 HV versus 198 HV for the as-sprayed state), owing to the increased fraction of Widmanstätten ferrite and the enhanced formation of harder Fe-rich intermetallic phases with additional passes.

3.4 Tribological Performance

3.4.1 Wear and Friction Coefficients. The wear test results for various samples are presented in Table 4. The friction coefficients for the different samples show negligible variation and range from 0.33 to 0.42. The low friction coefficient observed for the as-sprayed layer can be attributed to the porous structure of the Al-Fe coating (Ref 39, 40)

Figure 9 depicts the friction coefficients as a function of sliding distance. The sample subjected to three FSP passes exhibited fewer fluctuations compared to the other FSPed samples, which can be attributed to its homogenous structure resulting from high-pass FSP. The friction coefficient curves can be divided into two stages: (1) running-in and (2) quasi-steady state. Although the steady-state friction coefficients are almost identical for all FSPed samples, the sliding distances required to attain a quasi-steady state friction (running-in stage) differ compared to stage 2. The reduction in friction coefficient during the first stage may be attributed to the shearing of oxide layers at the contact interface. Oxide layers with lower shear strength exhibit greater lubricity. Once the steady state is reached, wear debris generated during sliding increases the contact area and leads to higher friction. Additionally, the formation of wear debris induces a transition from two-body to three-body wear mechanisms (Ref 40–42). Increasing the number of FSP passes results in a shorter running-in stage. Figure 3(a) indicates that an increase in pass number results in the formation of more intermetallic compounds on the surface. The presence of a greater amount of intermetallic compounds leads to a decrease in the proportion of pure Al on the surface, which reduces the oxidizing tendency. Additionally, EDS analysis of the wear debris (as shown in Fig. S4) demonstrated that the amount of oxygen decreases with an increase in pass number. Consequently, thinner oxide films are formed, resulting in a shorter running-in stage. The friction coefficients of heat-treated samples attained a quasi-steady state after a short sliding distance, as illustrated in Fig. S5.

Table 4 Wear test results of the as-sprayed coating, FSPed samples and heat-treated samples

Sample	Friction coefficient	Wear track depth, μm	Total wear rate, $\times 10^{-2}$, $\mu m^3\ m^{-1}$
As-sprayed coating	0.35	160±6	1.6±0.10
1 pass	0.41	152±5	1.4±0.15
2 pass	0.37	120±2	1.1±0.10
3 pass	0.42	18±3	0.15±0.02
4 pass	0.37	20±3	0.17±0.03
1 h-HT	0.33	140±2	1.3±0.10
2 h-HT	0.33	121±4	1.1±0.10

Figure 10 displays the weight loss variations of the heat-treated and FSPed samples subjected to a reciprocating wear test (for a sliding distance of 1000 m) under dry sliding conditions. The curves demonstrate that FSPed samples experienced lower weight loss compared to the as-sprayed Al-Fe coated sample. Among all the specimens, including heat-treated and other FSPed samples, those exposed to three and four FSP passes exhibited the lowest weight loss. The depth of penetration of reinforcement particles into the base substrate is known to increase with an increase in the number of FSP passes (Ref 43, 44). After a sliding distance of 300 m, the AISI 52100 pin of the second pass FSPed sample reached a depth from the surface with a low density of reinforcement particles. This led to a sharp increase in weight loss, as illustrated in Fig. 10. During the first 300 m of sliding, the weight loss of samples subjected to three and four FSP passes was much lower than during the subsequent 700 m of sliding.

Figure 11 displays the wear tracks obtained from a profilometer to calculate the total wear rate. The wear tracks produced on the surfaces of samples subjected to three and four FSP passes are shallower compared to the other samples. Additionally, the roughness of the worn surfaces for these two samples is comparatively smaller. The observed low roughness indicates a homogenous microstructure for the FSPed samples subjected to more FSP passes.

The results presented in Table 4 indicate that the samples fabricated using three and four FSP passes exhibit the lowest wear rates, which are almost ten times lower than the wear rate of the as-sprayed coatings. According to Table 4, the wear rate decreases from 1.6 $\times 10^{-2}$ $\mu m\ m^{-1}$ for the as-sprayed coating to 0.15 $\times 10^{-2}$ $\mu m\ m^{-1}$ and 0.17 $\times 10^{-2}$ $\mu m\ m^{-1}$ for the three- and four-pass samples, respectively. These values represent nearly an order of magnitude reduction in wear rate compared to the as-sprayed condition, confirming the substantial improvement achieved through multi-pass FSP. The differences in wear behavior among the different samples can be attributed to the variations in microstructure, hardness, and phase components resulting from FSP. The wear tracks produced on the surface of the samples subjected to three and four FSP passes have depths of 18 and 20 μm, respectively. At this depth of the wear track, the cross sectioned samples (Fig. 5k and n) exhibit a uniform distribution of the reinforcement particles in the microstructure. Additionally, numerous intermetallic compounds are formed in this layer. The wear tests demonstrated that the sample subjected to a 2 h heat treatment exhibited superior wear resistance compared to the sample that underwent 1 h heat treatment. In particular, the wear rate decreased from 1.3 $\times 10^{-2}$ $\mu m\ m^{-1}$ for the 1 h heat-treated sample to 1.1 $\times 10^{-2}$ $\mu m\ m^{-1}$ for the 2 h heat-treated sample. This could be attributed to the specific phases that formed during the heat treatment process. The XRD analysis presented in Fig. 3(b) shows the presence of Al_2O_3 phase in the sample treated for 2 h. This oxide phase contributes to an increase in the surface hardness and a decrease in the metal-metal contact, ultimately leading to improved wear resistance. The positive effects of Al_2O_3 in enhancing the tribological performance of Al-Fe composite coatings have also been reported in previous studies (Ref 44, 45). The improved wear resistance of the 2 h heat-treated sample can be attributed not only to the formation of the Al_2O_3 phase but also to the presence of the Fe_3Al (Fe-rich compound) phase at the surface. Overall, among all investi-

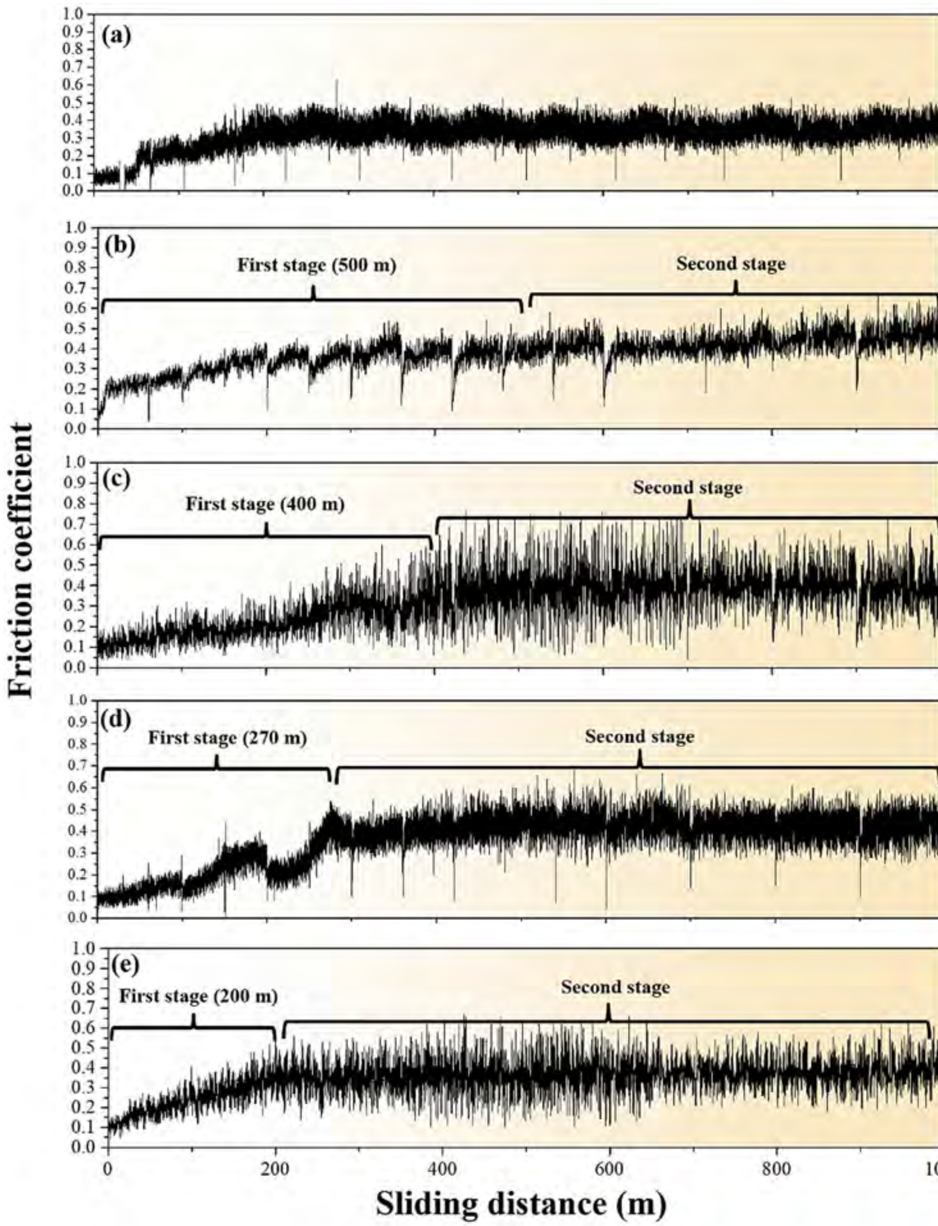

Fig. 9 Friction curves of (a) as-sprayed Al-Fe coating, and the surface composites fabricated by (b) one FSP pass, (c) two FSP passes, (d) three FSP passes, and (e) four FSP passes

gated conditions, the sample processed with three FSP passes exhibited the best wear performance, presenting the lowest wear rate (0.15×10^{-2} μm m^{-1}) in Table 4.

3.4.2 Worn Surfaces and Wear Mechanisms. To analyze the predominant wear mechanisms, the topographies of the worn surfaces were examined after the reciprocating wear test, and the results are presented in Fig. 12. The wear scars on these surfaces indicate that the primary wear mechanism for the as-sprayed coating is abrasive-type wear, which is accompanied by surface delamination, as shown in Fig. 12(a). The presence of porosity in as-sprayed coatings has been reported to increase the potential initiation sites for delamination and stress concentration. (Ref 40). The worn surfaces of the samples subjected to one and two FSP passes show adhesive-type wear as the dominant wear mechanism, as evidenced by the presence of welded points (Ref 46) (Fig. 12b and c). By increasing the number of FSP passes, the surface damage is reduced, and adhesive wear characteristics are significantly decreased, particularly for the samples subjected to three and four FSP passes. The two samples subjected to three and four FSP passes exhibit dominant abrasive-type wear mechanisms, with some plastic deformation also present in the worn surface of the latter (Fig. 12d and e). This wear mechanism is confirmed by the presence of striations on the worn surface (Ref 46). The worn surface of the sample subjected to the third FSP pass showed slight plowing, indicating the best wear performance compared to all FSPed and heat-treated samples (as seen in Fig. 12f and g). By increasing the pass number during FSP, the homogenous distribution of refined reinforcement particles was achieved (Ref 46-48), which may increase the pinning effect. As a result,

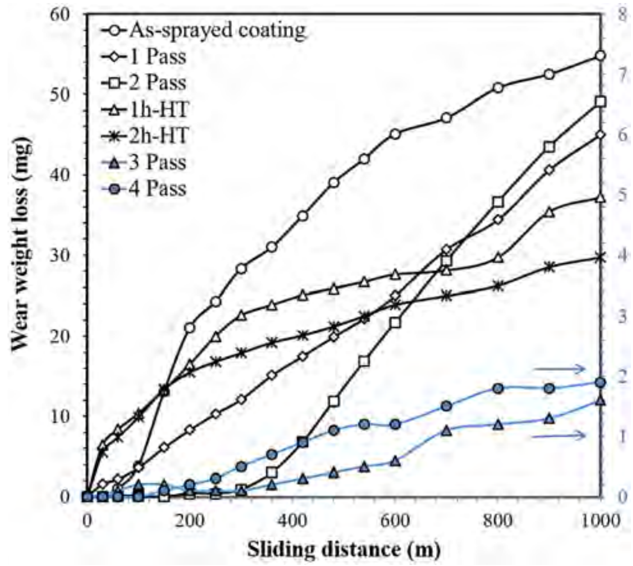

Fig. 10 Weigh losses of the samples as a function of *d* (sliding distance) in the linear reciprocating wear test

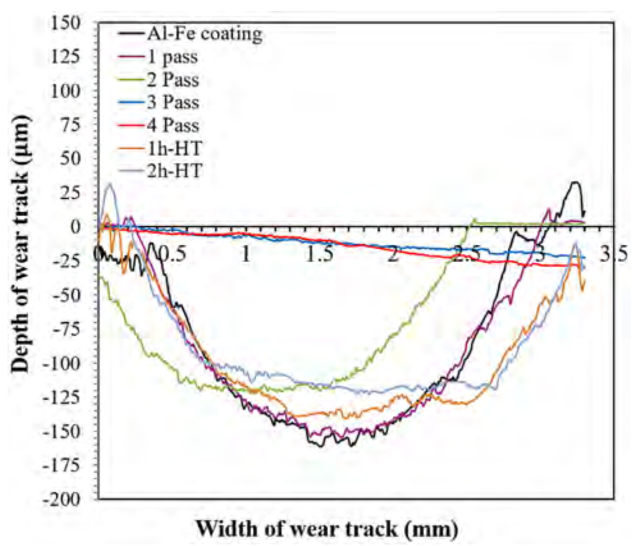

Fig. 11 Profilometry graphs of wear tracks of the Al-Fe as-sprayed, FSPed and heat-treated samples after the linear reciprocating wear test for a sliding distance of 1000 m

plowing resistance was enhanced by decreasing the lubrication effect and increasing the shear force generated from the pinned spots (Ref 49). In addition, Fe-rich intermetallic compounds were formed in the SZs as reported in the previous section. These Fe-rich iron aluminides have higher hardness and strength compared to Al-rich compounds (Ref 50), which could also contribute to the improved wear performance of samples subjected to three and four FSP passes.

4. Conclusion

The present research examined how the number of FSP passes impacted the microstructure, micro-hardness, and wear performance of an Al-Fe-coated low carbon steel. To summarize the findings:

1) The study showed that in situ fabrication of Fe-Al intermetallic compounds is possible using FSP. Increasing the number of FSP passes results in the creation of a greater number of stable intermetallic compounds.
2) The FSPed surfaces exhibited four distinct regions, namely SZ, CGHAZ, FGHAZ, and ICHAZ, each displaying a unique microstructure. Upon application of the second FSP pass, the recrystallized austenite grains underwent a transformation into Widmänstatten, polygonal, allotriomorphic ferrites, and degenerated pearlite colonies. With an increase in the number of FSP passes, the Widmanstätten grains underwent elongation and their volume fraction increased due to higher heat input and increased anisotropy of the structure, resulting from high dislocation density. The microstructure of CGHAZs was found to be almost identical to that of the SZs for each sample. Equiaxed fine ferrite grains were formed in FGHAZ.
3) The wear resistance of FSPed samples was significantly enhanced by increasing the number of passes, primarily due to improvements in surface hardness, uniform dispersion of reinforcement particles, and the formation of Fe-rich intermetallic compounds.
4) The friction coefficients of all samples were found to range between 0.33 and 0.42. The porous microstructure of the as-sprayed layer may have contributed to the low friction coefficient. Despite generating a more compact microstructure, FSP did not produce a significant difference in friction coefficients across the various samples. Increasing the number of passes resulted in a shorter running-in stage in FSPed samples due to the formation of fewer oxide phases on the surface during the reciprocating wear test.
5) XRD analysis revealed a gradual transition from Al-rich intermetallic compounds ($Al_{13}Fe_4$ and Al_5Fe_2) after the first pass toward Fe-rich phases such as Fe_3Al after multiple passes, confirming enhanced interfacial reactions due to cumulative heat input.
6) The disappearance of pure Al diffraction peaks after two or more passes indicates nearly complete intermetallic transformation, demonstrating the efficiency and repeatability of the multi-pass FSP process.
7) Quantitatively, the Vickers microhardness increased from 198 HV in the as-sprayed condition to 405 HV after four passes, representing more than a twofold improvement due to grain refinement, intermetallic formation, and increased dislocation density.
8) The total wear rate decreased from 1.6 $\times 10^{-2}$ $mm^3\,m^{-1}$ in the As-sprayed coating to 0.15 $\times$ 10^{-2} and 0.17 $\times 10^{-2}$ $mm^3\,m^{-1}$ after three and four passes, respectively, corresponding to nearly an order-of-magnitude enhancement in wear resistance.
9) The wear track depth was reduced from approximately 160 μm in the As-sprayed condition to 18-20 μm after three and four passes, confirming the formation of a dense and mechanically stable processed layer.
10) The strong agreement between phase evolution, microstructural observations, hardness measurements, and tribological data demonstrates that the multi-pass

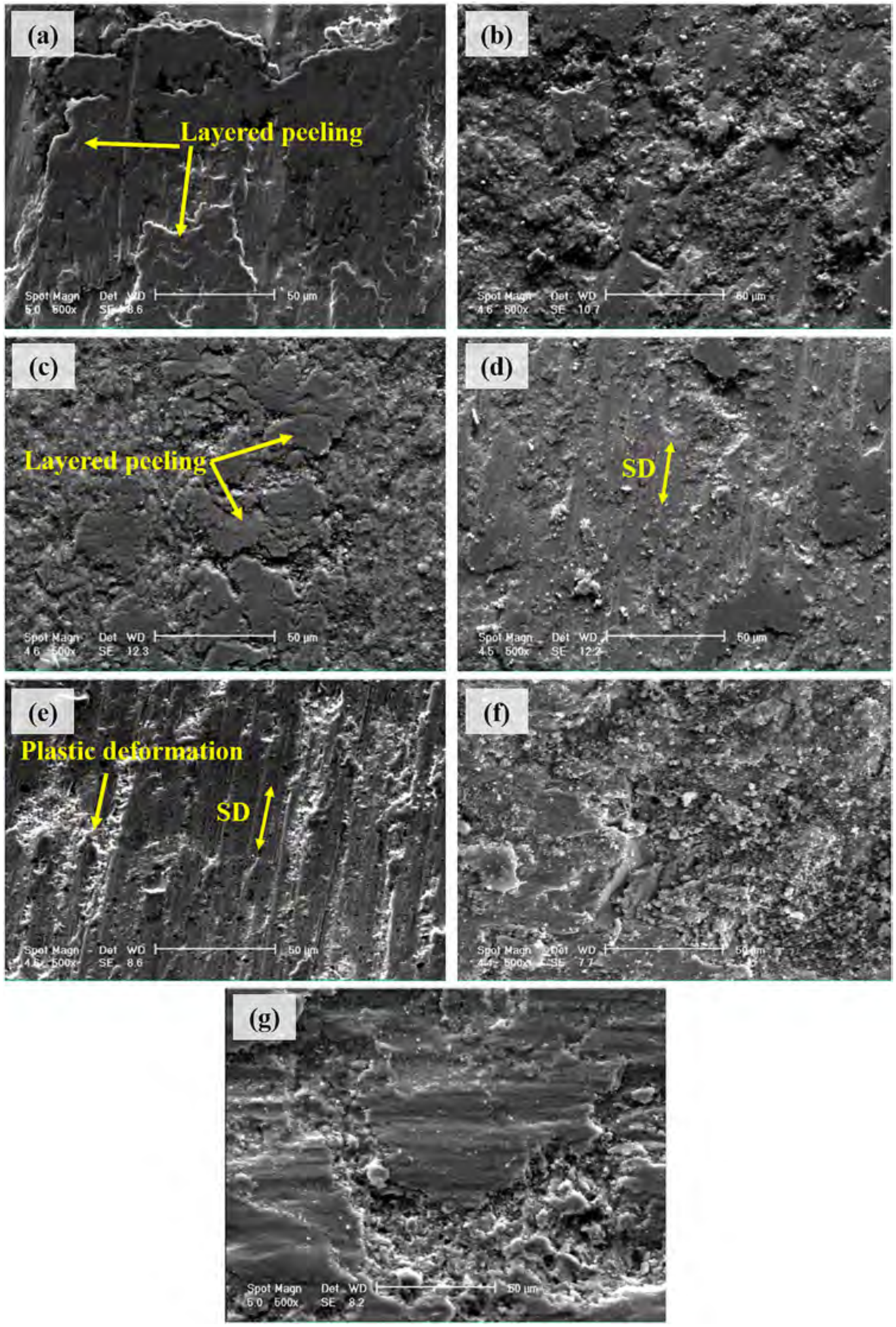

Fig. 12 SEM images of worn surfaces after 1000 m of AISI 52100 pin sliding during reciprocating wear test for: (a) Al-Fe coating, (b) first FSP pass, (c) second FSP pass, (d) third FSP pass, (e) fourth FSP pass, (f) 1 h-HT, and (g) 2 h-HT (SD indicates sliding direction)

FSP methodology provides a reliable and controllable approach for tailoring surface performance.

11) Although the highest hardness (405 HV) was achieved after four FSP passes, the lowest wear rate (0.15×10^{-2} mm^3 m^{-1}) was obtained after three passes, indicating that the three-pass condition provides the optimum balance between hardness and wear resistance.

Funding

Open access funding provided by Politecnico di Torino within the CRUI-CARE Agreement.

References

1. M.K. Gupta, Analysis of Tribological Behavior of Al/Gr/MoS2 Surface Composite Fabricated by Friction Stir Process, *Carbon Lett.*, 2020, **30**, p 399–408. https://doi.org/10.1007/s42823-019-00109-w
2. B. Sattari, M. Shamanian, F. Salimijazi, and M. Salehi, Surface Modification by Friction Stir Processing of Low-Carbon Steel: Microstructure Investigation and Wear Performance, *J. Mater. Eng. Perform.*, 2018, **27**, p 751–763. https://doi.org/10.1007/s11665-017-3087-7
3. X. Yang, Z. Yan, P. Dong, B. Cheng, J. Zhang, T. Zhang, H. Zhang, and W. Wang, Surface Modification of Aluminum Alloy by Incorporation of AlCoCrFeNi High Entropy Alloy Particles via Underwater Friction Stir Processing, *Surf. Coat. Technol.*, 2020, **385**, p 125438. https://doi.org/10.1016/j.surfcoat.2020.125438
4. M. Vakili-Azghandi, M. Roknian, J.A. Szpunar, and S.M. Mousavizade, Surface Modification of Pure Titanium via Friction Stir Processing: Microstructure Evolution and Dry Sliding Wear Performance, *J. Alloys Compd.*, 2020, **816**, p 152557. https://doi.org/10.1016/j.jallcom.2019.152557
5. K. Adiga, M.A. Herbert, S.S. Rao, and A.K. Shettigar, Optimization of Process Parameters for Friction Stir Processing (FSP) of AA8090/boron Carbide Surface Composites, *Weld. World*, 2024, **68**, p 2683–2700. https://doi.org/10.1007/s40194-024-01811-8
6. E.B. Moustafa, W.S. Abushanab, E.I. Ghandourah, M.A. Taha, and A.O. Mosleh, Advancements in Surface Reinforcement of AA2024 Alloy Using Hybridized Niobium Carbide and Ceramics Particles via FSP Technique, *Met. Mater. Int.*, 2024, **30**, p 800–813. https://doi.org/10.1007/s12540-023-01541-4
7. V. Sharma, U. Prakash, and B.V.M. Kumar, Surface Composites by Friction Stir Processing: A Review, *J. Mater. Process. Technol.*, 2015, **224**, p 117–134. https://doi.org/10.1016/j.jmatprotec.2015.04.019
8. H. Tanigawa, K. Ozawa, Y. Morisada, S. Noh, and H. Fujii, Modification of Vacuum Plasma Sprayed Tungsten Coating on Reduced Activation Ferritic/Martensitic Steels by Friction Stir Processing, *Fusion Eng. Des.*, 2015, **98–99**, p 2080–2084. https://doi.org/10.1016/j.fusengdes.2015.04.059
9. M. Paidar, O.O. Ojo, H.R. Ezatpour, and A. Heidarzadeh, Influence of Multi-pass FSP on the Microstructure, Mechanical Properties and Tribological Characterization of Al/B4C Composite Fabricated by Accumulative Roll Bonding (ARB), *Surf. Coat. Technol.*, 2019, **361**, p 159–169. https://doi.org/10.1016/j.surfcoat.2019.01.043
10. Y. Morisada, H. Fujii, T. Mizuno, G. Abe, T. Nagaoka, and M. Fukusumi, Modification of Thermally Sprayed Cemented Carbide Layer by Friction Stir Processing, *Surf. Coat. Technol.*, 2010, **204**, p 2459–2464. https://doi.org/10.1016/j.surfcoat.2010.01.021
11. C. Li, X. Feng, Y. Shen, and W. Chen, Preparation of Al_2O_3/TiO_2 Particle-Reinforced Copper Through Plasma Spraying and Friction Stir Processing, *Mater. Des.*, 2016, **90**, p 922–930. https://doi.org/10.1016/j.matdes.2015.11.047
12. N. Pol, G. Verma, R.P. Pandey, and T. Shanmugasundaram, Fabrication of AA7005/TiB_2-B_4C Surface Composite by friction Stir Processing: Evaluation of Ballistic Behaviour, *Def. Technol.*, 2019, **15**, p 363–368. https://doi.org/10.1016/j.dt.2018.08.002
13. R. Butola, Q. Murtaza, and R.M. Singari, Formation of Self-Assembled Monolayer and Characterization of AA7075-T6/B4C Nano-Ceramic Surface Composite Using Friction Stir Processing, *Surf. Topogr.: Metrol. Prop.*, 2020, **8**, p 025030. https://doi.org/10.1088/2051-672X/ab96db
14. S.K. Patel, V.P. Singh, and B. Kuriachen, in *Modification of Aluminium Alloy Surface Composite Reinforced with* ZrO_2 *Particles Fabricated Through Friction Stir Processing*, ed. by M. Shunmugam and M. Kanthababu. Advances in Additive Manufacturing and Joining (Springer, 2020), p 545–554. https://doi.org/10.1007/978-981-32-9433-2_50
15. M. Barati, M. Abbasi, and M. Abedini, The Effects of Friction Stir Processing and Friction Stir Vibration Processing on Mechanical, Wear and Corrosion Characteristics of Al6061/SiO_2 Surface Composite, *J. Manuf. Process.*, 2019, **45**, p 491–497. https://doi.org/10.1016/j.jmapro.2019.07.034
16. Y. Yang, M. Paidar, S. Mehrez, and O.O. Ojo, Enhancement of Mechanical Properties and Wear of AA5083/316 Stainless Steel Surface-Composite Developed Through Multi-pass Friction Stir Processing (MPFSP), *Arch. Civ. Mech. Eng.*, 2022, **23**, p 13. https://doi.org/10.1007/s43452-022-00556-9
17. G. Huang, W. Hou, J. Li, and Y. Shen, Development of Surface Composite Based on Al-Cu System by Friction Stir Processing: Evaluation of Microstructure, Formation Mechanism and Wear Behavior, *Surf. Coat. Technol.*, 2018, **344**, p 30–42. https://doi.org/10.1016/j.surfcoat.2018.03.005
18. S. Zhang, Y. Li, A. Frederick, Y. Wang, Y. Wang, L. Allard, M. Koehler, S. Shin, A. Hu, and Z. Feng, In-situ Formation of Al3Ni Nano Particles in Synthesis of Al 7075 Alloy by Friction Stir Processing with Ni Powder Addition, *J. Mater. Process. Technol.*, 2023, **311**, p 117803. https://doi.org/10.1016/j.jmatprotec.2022.117803
19. C. Huang, Y. Xia, C. Xia, and F. Liu, Double Reinforcement of Al-Fe Intermetallic Composites Fabricated by Friction Stir Processing, *Metals*, 2019, **9**, p 1002. https://doi.org/10.3390/met9091002
20. A. Heidarpour, Y. Mazaheri, M. Roknian, and S. Ghasemi, Development of Cu-TiO2 Surface Nanocomposite by Friction Stir Processing: Effect of Pass Number on Microstructure, Mechanical Properties, Tribological and Corrosion Behavior, *J. Alloys Compd.*, 2019, **783**, p 886–897. https://doi.org/10.1016/j.jallcom.2018.12.382
21. V. Singhal, V.K. Jain, R.S. Raman, D. Patharia, V. Mittal, S. Mishra, and H. Kumar, Optimization of Friction Stir Processing Parameters for Improving Structural and Mechanical Properties in in situ AA5083-H111/Al-Fe Composites, *Proc. Inst. Mech. Eng. C J. Mech. Eng. Sci.*, 2024, **238**, p 4477–4490. https://doi.org/10.1177/09544062231211672
22. S. Saravanakumar, K.B. Prakash, D. Dinesh, P. Manoj Kumar, Y. Fouad, M.E.M. Soudagar, M.M. Ali, and M.N. Bashir, Optimizing Friction Stir Processing Parameters for Aluminium Alloy 2024 Reinforced with SiC Particles: A Taguchi Approach of Investigation, *J. Mater. Res. Technol.*, 2024, **30**, p 4847–4855. https://doi.org/10.1016/j.jmrt.2024.04.066
23. R. Senthilkumar, M. Prakash, N. Arun, and A.A. Jeyakumar, The Effect of the Number of Passes in Friction Stir Processing of Aluminum Alloy (AA6082) and its Failure Analysis, *Appl. Surf. Sci.*, 2019, **491**, p 420–431. https://doi.org/10.1016/j.apsusc.2019.06.132
24. B. Sattari, M. Shamanian, A. Ashrafi, M. Salehi, and F. Salimijazi, Effect of Number of Passes on the Corrosion Behavior of Fe/Al Surface Composites Produced by Plasma Spraying and Friction Stir Processing, *J. Mater. Process. Technol.*, 2017, **250**, p 35–44. https://doi.org/10.1016/j.jmatprotec.2017.06.018
25. V. Malik and S.V. Kailas, Understanding the Effect of Tool Geometrical Aspects on Intensity of Mixing and Void Formation in Friction Stir Process, *Proc. Inst. Mech. Eng. C J. Mech. Eng. Sci.*, 2021, **235**, p 744–757. https://doi.org/10.1177/0954406220938410
26. L. Wan and Y. Huang, Friction Stir Welding of Dissimilar Aluminum Alloys and Steels: A Review, *Int. J. Adv. Manuf. Technol.*, 2018, **99**, p 1781–1811. https://doi.org/10.1007/s00170-018-2601-x
27. V. Singhal, V.K. Jain, R.S. Raman, D. Patharia, V. Mittal, S. Mishra, and H. Kumar, Optimization of Friction Stir Processing Parameters for Improving Structural and Mechanical Properties in in situ AA5083-H111/Al-Fe Composites, *Proc. Inst. Mech. Eng. C J. Mech. Eng. Sci.*, 2024, **238**, p 4477–4490. https://doi.org/10.1177/09544062231211672
28. C.J. Hsu, P.W. Kao, and N.J. Ho, Intermetallic-Reinforced Aluminum Matrix Composites Produced in situ by Friction Stir Processing, *Mater. Lett.*, 2007, **61**, p 1315–1318. https://doi.org/10.1016/j.matlet.2006.07.021

29. Y. Xue, R. Shen, S. Ni, M. Song, and D. Xiao, Fabrication, Microstructure and Mechanical Properties of Al-Fe Intermetallic Particle Reinforced Al-Based Composites, *J. Alloys Compd.*, 2015, **618**, p 537–544. https://doi.org/10.1016/j.jallcom.2014.09.009
30. N. Cinca, C.R.C. Lima, and J.M. Guilemany, An Overview of Intermetallics Research and Application: Status of Thermal Spray Coatings, *J. Mater. Res. Technol.*, 2013, **2**, p 75–86. https://doi.org/10.1016/j.jmrt.2013.03.013
31. R. Feng, S. Li, X. Zhu, and Q. Ao, Microstructural Characterization and Formation Mechanism of Abnormal Segregation Band of Hot Rolled Ferrite/Pearlite Steel, *J. Alloys Compd.*, 2015, **646**, p 787–793. https://doi.org/10.1016/j.jallcom.2015.05.128
32. W. Yan, N. Xiao, Y. Chen, and D. Li, Phase-Field Modeling of Widmanstätten Ferrite Formation During Isothermal Transformation in Low Carbon Steels, *Comput. Mater. Sci.*, 2014, **81**, p 503–509. https://doi.org/10.1016/j.commatsci.2013.09.001
33. J. Rodriguez and A.J. Ramirez, Microstructural Characterisation of Friction Stir Welding Joints of Mild Steel to Ni-Based Alloy 625, *Mater. Charact.*, 2015, **110**, p 126–135. https://doi.org/10.1016/j.matchar.2015.10.023
34. R. Grewal, C. Aranas, K. Chadha, D. Shahriari, M. Jahazi, and J.J. Jonas, Formation of Widmanstätten Ferrite at Very High Temperatures in the Austenite Phase Field, *Acta Mater.*, 2016, **109**, p 23–31. https://doi.org/10.1016/j.actamat.2016.02.062
35. M. Cottura, B. Appolaire, A. Finel, and Y. Le Bouar, Phase Field Study of Acicular Growth: Role of Elasticity in Widmanstätten Structure, *Acta Mater.*, 2014, **72**, p 200–210. https://doi.org/10.1016/j.actamat.2014.03.045
36. L. Zhang, Y. Shen, H. Wan, X. Xiong, and L. Zhang, The Study of Widmanstätten Ferrite in Fe-C Alloys by a Phase Field Model Coupled with Anisotropic Elasticity, *J. Alloys Compd.*, 2015, **650**, p 239–247. https://doi.org/10.1016/j.jallcom.2015.07.278
37. B. Li, Y. Shen, L. Luo, and W. Hu, Fabrication of TiCp/Ti-6Al-4V Surface Composite via Friction Stir Processing (FSP): Process Optimization, Particle Dispersion-Refinement Behavior and Hardening Mechanism, *Mater. Sci. Eng. A*, 2013, **574**, p 75–85. https://doi.org/10.1016/j.msea.2013.03.019
38. L. Cheng, K.M. Wu, X.L. Wan, and R. Wei, In-situ Observation on the Growth of Widmanstätten Sideplates in an Fe-C-Mn Steel, *Mater Charact*, 2014, **87**, p 86–94. https://doi.org/10.1016/j.matchar.2013.11.002
39. C. Langlade, A. Roman, D. Schlegel, E. Gete, and M. Folea, Formation of a Tribologically Transformed Surface (TTS) on AISI 1045 Steel by Friction Stir Processing, *Mater. Manuf. Processes*, 2016, **31**, p 1565–1572. https://doi.org/10.1080/10426914.2015.1090584
40. A. Rahbar-kelishami, A. Abdollah-zadeh, M.M. Hadavi, R.A. Seraj, and A.P. Gerlich, Improvement of Wear Resistance of Sprayed Layer on 52100 Steel by Friction Stir Processing, *Appl. Surf. Sci.*, 2014, **316**, p 501–507. https://doi.org/10.1016/j.apsusc.2014.08.033
41. C. Bidmeshki, V. Abouei, H. Saghafian, S.G. Shabestari, and M.T. Noghani, Effect of Mn Addition on Fe-Rich Intermetallics Morphology and Dry Sliding Wear Investigation of Hypereutectic Al-17.5%Si Alloys, *J. Mater. Res. Technol.*, 2016, **5**, p 250–258. https://doi.org/10.1016/j.jmrt.2015.11.008
42. H. Sarmadi, A.H. Kokabi, and S.M. Seyed Reihani, Friction and Wear Performance of Copper–Graphite Surface Composites Fabricated by Friction Stir Processing (FSP), *Wear*, 2013, **304**, p 1–12. https://doi.org/10.1016/j.wear.2013.04.023
43. P.V. Moghaddam, M. Rinaudo, J. Hardell, E. Vuorinen, and B. Prakash, Influence of Fracture Toughness on Two-Body Abrasive Wear of Nanostructured Carbide-Free Bainitic Steels, *Wear*, 2020, **460–461**, p 203484. https://doi.org/10.1016/j.wear.2020.203484
44. M. Rahsepar and H. Jarahimoghadam, The Influence of Multipass Friction Stir Processing on the Corrosion Behavior and Mechanical Properties of Zircon-Reinforced Al Metal Matrix Composites, *Mater. Sci. Eng. A*, 2016, **671**, p 214–220. https://doi.org/10.1016/j.msea.2016.05.056
45. H. Seifiyan, M. Heydarzadeh Sohi, M. Ansari, D. Ahmadkhaniha, and M. Saremi, Influence of Friction Stir Processing Conditions on Corrosion Behavior of AZ31B Magnesium Alloy, *J. Magnesium Alloys*, 2019, **7**, p 605–616. https://doi.org/10.1016/j.jma.2019.11.004
46. R. Hashemi and G. Hussain, Wear Performance of Al/TiN Dispersion Strengthened Surface Composite Produced Through Friction Stir Process: A Comparison of Tool Geometries and Number of Passes, *Wear*, 2015, **324–325**, p 45–54. https://doi.org/10.1016/j.wear.2014.11.024
47. B. Song, S. Dong, H. Liao, and C. Coddet, Microstructure and Wear Resistance of FeAl/Al_2O_3 Intermetallic Composite Coating Prepared by Atmospheric Plasma Spraying, *Surf. Coat. Technol.*, 2015, **268**, p 24–29. https://doi.org/10.1016/j.surfcoat.2014.06.055
48. C. Huang, W. Li, Z. Zhang, M. Fu, M. Planche, H. Liao, and G. Montavon, Modification of a Cold Sprayed SiCp/Al5056 Composite Coating by Friction Stir Processing, *Surf. Coat. Technol.*, 2016, **296**, p 69–75. https://doi.org/10.1016/j.surfcoat.2016.04.016
49. N. Gangil, S. Maheshwari, and A.N. Siddiquee, Multipass FSP on AA6063-T6 Al: Strategy to Fabricate Surface Composites, *Mater. Manuf. Processes*, 2018, **33**, p 805–811. https://doi.org/10.1080/10426914.2017.1415448
50. M. Krasnowski and T. Kulik, Nanocrystalline Al-Fe Intermetallics–Light Weight Alloys with High Hardness, *Intermetallics*, 2010, **18**, p 47–50. https://doi.org/10.1016/j.intermet.2009.06.006